Using Three-Pulse Femtosecond Spectroscopy to Probe Ultrafast Triplet Energy Transfer in Zinc *meso*-Tetraarylporphyrin−Perylene-3,4-dicarboximide Dyads

Ryan T. Hayes, Christopher J. Walsh, and Michael R. Wasielewski*

Department of Chemistry and Center for Nanofabrication and Molecular Self-Assembly, Northwestern University, Evanston, Illinois 60208-3113

Received: July 14, 2003; In Final Form: February 11, 2004

Linear arrays of zinc *meso*-tetraarylporphyrin (ZnP), perylene-3,4-dicarboximide (PMI), and either naphthalene-1,8:4,5-bis(dicarboximide) (NI) or pyromellitimide (PI) were synthesized and studied by ultrafast transient absorption spectroscopy. PMI was covalently linked in one of two orientations relative to ZnP. In one set of molecules, the 9 position of the perylene core is connected to the *para* position of a *meso*-phenyl in ZnP to give ZnP−PMI−*N*−X, where X = NI or PI is attached to the imide nitrogen atom of PMI. In the second set of compounds, the imide nitrogen atom of PMI is connected to the *meso*-phenyl in ZnP to give ZnP−*N*−PMI−X, where X = PI or H. Selective excitation of ZnP using 420 nm, 110 fs laser pulses in each molecule in toluene produces ^{1*}ZnP, which intersystem crosses (ISC) to ^{3*}ZnP with $\tau = 2.3$ ns. For ZnP−PMI−*N*−X, triplet energy transfer (TET) from ^{3*}ZnP to PMI is much faster than ISC, so that ^{3*}ZnP is not observed by one-pump−one-probe transient absorption spectroscopy. Following its formation, the lowest excited triplet state of ^{3*}PMI was excited with a 575 nm, 110 fs laser pulse to produce an upper excited triplet state, ^{3**}PMI. In ZnP−PMI−*N*−X, subpicosecond TET from ^{3**}PMI re-populates ^{3*}ZnP, which subsequently undergoes TET back to PMI with a rate of $(7\text{ ps})^{-1}$. The same experiment carried out on ZnP−*N*−PMI−X reveals that the TET process ^{3*}ZnP−*N*−PMI−X → ZnP−^{3*}*N*−PMI−X occurs with a rate of $(55\text{ ns})^{-1}$. The nearly 8000-fold larger TET rate from ^{3*}ZnP to PMI in ZnP−PMI−*N*−X relative to that in ZnP−*N*−PMI−X is a consequence of the larger π-orbital coefficients at the 9 position in both the HOMO and LUMO of PMI relative to that on its imide nitrogen atom. This basic asymmetry allows optimization of energy and electron and/or hole transfer rates in large assemblies containing PMI for use in organic molecular electronics.

Introduction

Two-pump (two-color or stepwise excitation) pulsed laser techniques have shown that photoionization, bond cleavage, isomerization, energy transfer, and electron transfer within organic chromophores often involve higher electronic states of singlet,[1,2] triplet,[2−6] and radical ion[3−5] states. Two-pump, one-probe spectroscopy has also been used to control electron and energy transfer within linear and branch arrays of organic chromophores for approaches to optically controlled molecular switches.[7] Recently, the novel use of perylene-3,4-dicarboximides (PMI) as antenna chromophores to transfer energy to zinc porphyrins (ZnP) has been reported.[8−10] In one of these reports, one-pump transient absorption spectroscopy was used to determine that singlet energy transfer from ^{1*}PMI to ZnP in zinc *meso*-tetraarylporphyrin-ethynylphenyl-perylene-3,4-dicarboximide (ZnP-ep-PMI),[10] occurs very rapidly with a rate constant of $(0.4\text{ ps})^{-1}$. In addition, it was reported that intersystem crossing of ^{1*}ZnP to ^{3*}ZnP is followed by very rapid triplet energy transfer (TET) to PMI, which occurs at a rate much faster than the $(2.3\text{ ns})^{-1}$ ISC rate of ZnP. Although a rate was not established for fast TET for ^{3*}ZnP−ep−PMI → ZnP−ep−^{3*}PMI in this report, it is useful to understand how PMI behaves as a triplet-energy acceptor since PMI has been established as an important light harvesting pigment for porphyrins[8−10] and as a photoactive component in electron donor−acceptor molecules.[11−16]

PMI is readily functionalized at its 9-position and at the nitrogen atom of its 3,4-dicarboximide. Semiempirical electronic structure calculations[17] show that both the HOMO and LUMO of PMI have a nodal plane that bisects the long axis of the molecule and includes the nitrogen atom of the imide group. For example, the π orbital coefficients on the 9-carbon atom of 1,6-diphenoxy−PMI are −0.1117 (HOMO) and 0.0884 (LUMO), whereas those on the imide nitrogen atom are −0.0004 (HOMO) and 0.0003 (LUMO).[18] TET is essentially a through-bond process that takes place via the Dexter mechanism, an electron−electron exchange interaction involving simultaneous hole and electron transfer between the donor and acceptor.[19,20] Consequently, the large difference between the π orbital coefficients of the 9-carbon atom and the imide nitrogen atom for both the HOMO and LUMO of PMI should result in large changes in TET rates depending on which position of PMI the ZnP triplet donor is attached. Similarly, electron-transfer reactions involving PMI will also exhibit position dependent rates because the electronic coupling matrix element for electron transfer also depends on orbital overlap at the point of attachment of the electron donor and acceptor.[21]

To understand how the orientation of PMI influences TET rates and how TET may compete with electron transfer, a series of linear arrays were synthesized with the electron acceptors, pyromellitimide (PI) or naphthalene-1,8:4,5-bis(dicarboximide) (NI). The molecules are divided into two groups based on how PMI is attached to the zinc porphyrin, Figure 1. The molecules in the first set have the 9 position of the perylene core connected

* To whom correspondence should be addressed. E-mail: wasielew@chem.northwestern.edu.

10.1021/jp0360319 CCC: $27.50
Published on Web 03/20/2004

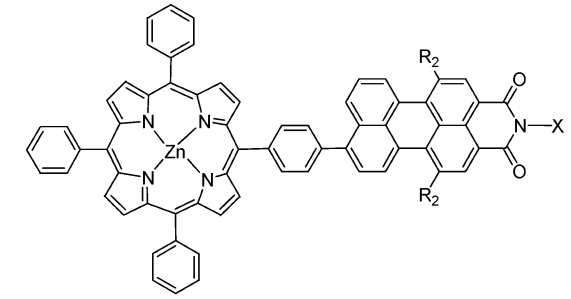

ZnP-PMI-*N*-X, X = NI, PI, t-Bu_2Ph

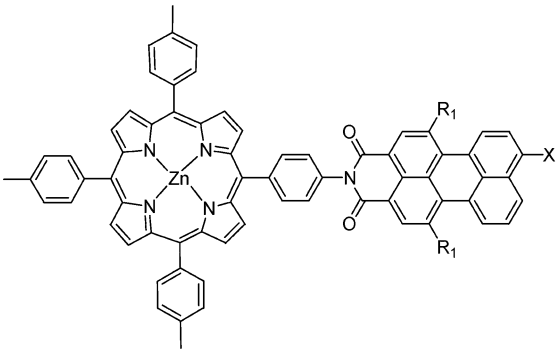

ZnP-*N*-PMI-X, X = H, PI

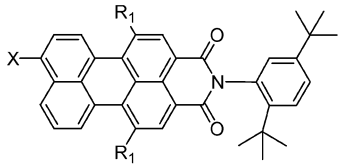

X-PMI-*N*-t-Bu_2Ph, X = Ph, PI

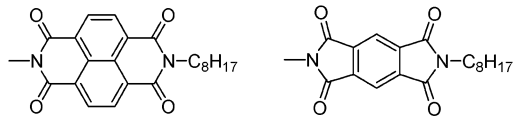

NI PI

Figure 1. Dyad and triads studied in this paper. R_1 = *p-tert*-butylphenoxy, R_2 = 3,5-di-*tert*-butylphenoxy.

to the para position of a *meso*-phenyl in ZnP to give ZnP−PMI−*N*−X, where X = NI or PI. In the second set of compounds, the nitrogen atom of PMI is connected to the para position of a *meso*-phenyl in ZnP in ZnP-*N*-PMI-X, where X = PI or H. Using three-pulse, i.e., two-pump, one-probe, femtosecond and nanosecond transient absorption experiments in toluene, we show that the TET rates from ZnP to PMI are very sensitive to whether ZnP is attached to the 9 position or the N-imide of PMI. For ^{3*}ZnP−PMI−*N*−X → ZnP−^{3*}PMI−*N*−X, the TET rate is $(7ps)^{-1}$ and is nearly 8000 times faster than the $(55ns)^{-1}$ TET rate for ^{3*}ZnP−*N*−PMI−X → ZnP−^{3*}*N*−PMI−X. Using structural differences to control TET rates to PMI should prove useful for developing strategies for molecular based electronics and light harvesting arrays with porphyrins.

Experimental Section

Syntheses of the molecules shown in Figure 1 are detailed in the Supporting Information. Femtosecond transient absorption measurements were made using a regeneratively amplified titanium sapphire laser system operating at a 2 kHz repetition rate outfitted with a CCD array detector (Ocean Optics PC2000) for simultaneous collection of spectral and kinetic data.[22] The frequency-doubled output from the laser provides 420 nm, 110 fs pulses for excitation, whereas 575 nm, 110 fs excitation pulses were produced using an optical parametric amplifier (OPA).[23] The tunable OPA pulses can be delayed by as much as 3.5 ns relative to the 420 nm pulse. Focusing a few microjoules of the 840 nm fundamental into a 1 mm sapphire disk generated a white light continuum probe pulse. Cuvettes with a 2 mm path length were used and the samples were irradiated with 0.7 μJ per pulse focused to a 200 μm spot. The optical density at the excitation wavelength was typically 0.2−0.6. The samples were stirred with a wire during the experiment to prevent thermal lensing and sample degradation. The total instrument response for the pump−probe experiments was 150 fs. The two-pump, one-probe femtosecond experiment has been described in detail previously.[24,25] Under these experimental conditions, a ZnP sample with about 0.5 absorbance at 420 nm in a 2 mm cuvette pumped with 0.7 μJ per pulse at 420 nm focused to a 200 μm spot has about 1.9×10^{11} molecules in the pumped volume and 1.5×10^{12} photons in the laser pulse pumping that volume. This results in a very high turnover of ground-state ZnP to ^{1*}ZnP, followed in turn by high yield formation of ^{3*}ZnP and ^{3*}PMI. High turnovers are easily achieved when molecules with large extinction coefficients are excited.[26] This produces a significant ^{3*}PMI absorption that absorbs most of the second pump pulse energy resulting in easily discernible absorption changes following the second pulse. The same is true for the nanosecond experiment described below. The stability of the molecules studied here is excellent, so that the high excited-state populations present during the experiment do not result in significant decomposition of the molecules over the course of the experiments as checked by UV-vis spectroscopy and MALDI-TOF on the samples after the data is collected.

One and two-pump pulse nanosecond transient absorption measurements were performed using a 10-Hz Nd:YAG laser system. The frequency tripled output, 355 nm, was directed through a high-pressure H_2-cell that generated Raman-shifted 416 nm, 7 ns pulses. For the second excitation pulse, the residual frequency-doubled 532 nm light was separated with a dichroic mirror and directed over a 27-m optical delay line resulting in a pump delay of 90 ns. A detailed explanation and illustration of the data collection for the two-pump nanosecond experiment is located in the Supporting Information. Samples for nanosecond spectroscopy were prepared in a 1 cm quartz vacuum cell and were deoxygenated using three freeze−pump−thaw cycles. The probe light in the nanosecond experiments was generated using a xenon flashlamp (EG&G Electrooptics FX-200, 50 μs pulse) and detected using a photomultiplier tube with high voltage applied to only 4 dynodes (Hamamatsu R928). All experiments were carried out in spectrophotometric grade toluene with a 0.2−0.6 optical density of absorbing chromophore at the excitation wavelength. The samples were checked by steady-state absorption before and after laser spectroscopy to ensure sample integrity.

Kinetic analyses were performed at several wavelengths using a nonlinear least-squares fit to either a general sum of exponentials function or to a series A → B → C kinetic mechanism using the Levenberg−Marquardt algorithm.

Steady-state absorption and emission spectra were obtained on a Shimadzu 1601 UV/vis spectrophotometer using a 10 mm path length quartz cuvette.

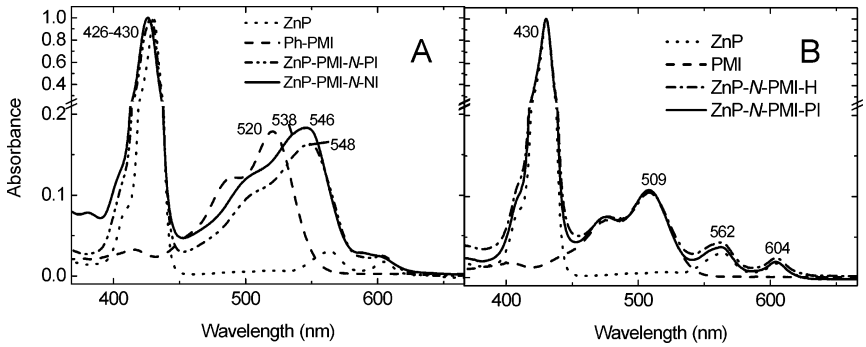

Figure 2. Ground-state absorption spectra in toluene normalized at the Soret band for (A) ZnP−PMI−*N*−X relative to Ph−PMI and ZnP, and (B) ZnP−*N*−PMI−X relative to PMI and ZnP.

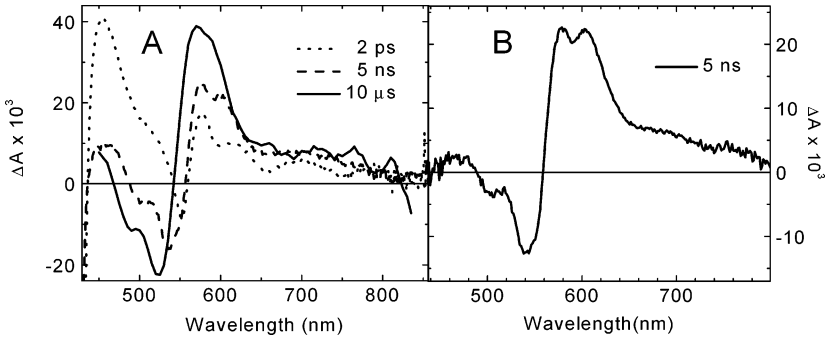

Figure 3. Transient absorption spectra in toluene following 420 nm, 110 fs excitation. (A) ZnP−PMI−*N*−NI and (B) ZnP−PMI−*N*−PI

Results and Discussion

Ground-State Absorption Spectroscopy. Figure 2A shows the ground-state absorption spectra of ZnP−PMI−*N*−X (X = PI or NI) in toluene. The ground-state absorption of PMI is red-shifted by 18 nm relative to that of Ph−PMI−*N*−(*t*-Bu_2-Ph). This result suggests that significant electronic interaction takes place between the porphyrin and perylene chromophores. This is consistent with the findings reported by Yang et al.[10] for ZnP−ep−PMI, which contains an ethynyl-phenyl spacer with the ethynyl group attached to the meso position of ZnP. We see the same ground state absorption spectrum for our system in which ZnP and PMI are separated by only a phenyl. Yang et al. conclude that this electronic interaction results from perturbation of the lowest excited singlet state of PMI by the porphyrin. In contrast, the ground-state absorption features of ZnP-*N*-PMI-X in toluene, Figure 2B, show that the electronic interaction between ZnP and PMI is relatively weak. The ground-state absorption spectrum of ZnP−*N*−PMI−X is equal to the sum of the ground-state absorption spectra of ZnP and PMI. This reduced electronic interaction is a result of the small π electron density on imide nitrogen atom joining ZnP and PMI in the ZnP−*N*−PMI−X compounds.

One-Pump−One-Probe Transient Absorption Spectroscopy. One-pump−one-probe transient absorption spectroscopy was performed on ZnP−PMI−*N*−NI in toluene. Figure 3A shows the transient absorption spectra after 420 nm, 110 fs excitation. At 2 ps, the characteristic absorption feature of ^{1*}ZnP appears at 460 nm along with the Q(1,0) and Q(0,0) ground-state absorption bleaches near 550 and 595 nm, respectively. The stimulated emission from Q(0,1) appears as a dip in the transient absorption at 650 nm. The transient absorption kinetics at 460 nm decay with a 2.3 ns time constant, which matches literature values for ^{1*}ZnP → ^{3*}ZnP intersystem crossing.[27] This indicates that electron transfer ^{1*}ZnP to PMI does not occur within ZnP−PMI−*N*−NI in toluene. Given that the one electron oxidation and reduction potentials of ZnP and PMI are 0.82 V[28] and −0.9 V[14] vs SCE, respectively, and the lowest excited singlet state energy of ZnP is 2.07 eV, the free energy for the reaction ^{1*}ZnP−PMI → ZnP^+−PMI^- in toluene is positive by 0.1−0.2 eV.[23] The transient absorption spectrum at 5 ns shows that a dramatic change has taken place with the 460 nm absorption replaced by two large bleaches at 500 and 538 nm, which correspond to ground-state depletion of PMI, and formation of a new absorption maximum at 575 nm. When a degassed sample of ZnP−PMI-*N*-NI is excited with 416 nm, 7 ns pump pulses, the transient spectrum at 10 μs shows that the 575 nm absorption persists at long times. Taking into consideration the long lifetime of this transient absorption feature, and the fact that ^{1*}ZnP−PMI−*N*−NI decays with a rate similar to that of ^{1*}ZnP itself, we assign this long-lived state to ^{3*}PMI. Since there is no evidence of a significant build-up ^{3*}-ZnP population in the one-pump transient absorption experiment, the results suggest that the TET rate from ^{3*}ZnP−PMI−*N*−NI → ZnP−^{3*}PMI−*N*−NI is much faster than the $(2.3\ \text{ns})^{-1}$ intersystem crossing rate of ^{1*}ZnP. The actual TET rate cannot be determined from the one-pump experiment but will be measured using the two-pump transient absorption experiment described below.

The corresponding one-pump transient absorption spectrum for ZnP−PMI−*N*−PI in toluene is shown in Figure 3B. The transient absorption spectra of ZnP−PMI−*N*−PI and ZnP−PMI−*N*−NI at 5 ns are very similar. The kinetics at 460 nm (^{1*}ZnP decay) and 575 nm (^{3*}PMI formation) are monoexponential with time constants of 2.3 ns. The transient spectra and kinetics suggest that charge separation does not occur within ZnP−PMI−*N*−PI. Once again, the TET process, ^{3*}ZnP−PMI−*N*−PI → ZnP-^{3*}PMI−*N*−PI, is too fast to measure in the one-pump experiment.

Excitation of ZnP−*N*−PMI−PI using 420 nm pulses yields a transient absorption spectrum at 50 ps, Figure 4A, which corresponds to that of ^{1*}ZnP as described above. Very similar data are obtained for ZnP−*N*−PMI−H (not shown). After 6

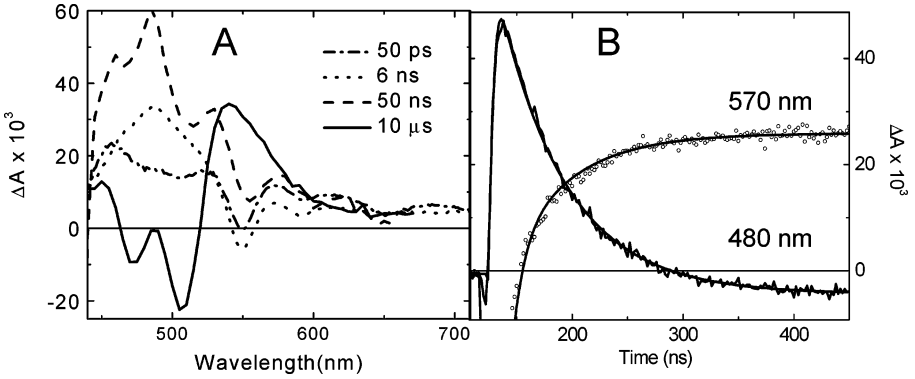

Figure 4. Transient absorption data of ZnP−*N*−PMI−PI following one-pump, 420 nm excitation in toluene. (A) Transient absorption spectra. The 50 ns and 10 μs spectra are results from the nanosecond experiment using 416 nm, 7 ns pump pulses. (B) Transient absorption kinetics for ZnP−*N*−PMI−PI from the one-pump, 416 nm nanosecond experiment.

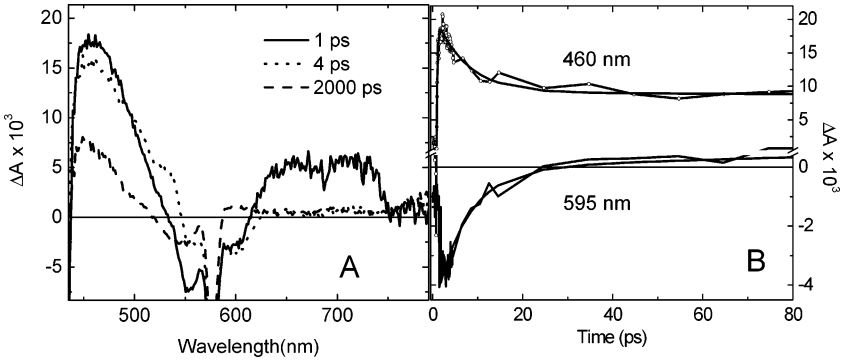

Figure 5. (A) Two-pulse−one-probe femtosecond spectra for ZnP−PMI−*N*−NI in toluene. The sample is excited at $t = 0$ with a 420 nm, 110 fs pulse at repetition frequency ω, followed by a second 575 nm, 110 fs pulse at $t = 3.5$ ns at repetition frequency $\omega/2$. The sharp negative feature at 575 nm is scattered pump light. (B) Transient absorption kinetics obtained at 460 and 595 nm. The abcissa gives the time following the 575 nm pulse.

ns, Figure 4A shows transient absorption features that are typical of ^{3*}ZnP [29−31] with an intense band around 485 nm and a small, broad absorption from 600 to 750 nm. Using a 416 nm, 7 ns pump, the transient absorption spectrum of ^{3*}ZnP at 485 nm ($\tau_{decay} = 55$ ns, Figure 4B) is replaced by a spectrum having an absorption at 540 nm ($\tau_{rise} = 55$ ns, Figure 4B) with two bleaches at 470 and 510 nm, which correspond to ground-state depletion of PMI. The 540 nm absorption feature persists in a degassed solution for times >50 μs. These long-lived spectral changes are assigned to the formation of ^{3*}PMI.

Two-Pump−One-Probe Femtosecond Transient Absorption Spectroscopy. Two-pump−one-probe femtosecond transient absorption spectroscopy was performed on ZnP−PMI−*N*−X using a 420 nm initial excitation pulse followed by 3.5 ns delay and then application of a second 575 nm pump pulse. The delay was selected to provide sufficient time for the formation of ZnP−^{3*}PMI−*N*−NI as the major species. In this experiment, one pump beam is chopped at $\omega/2$, where ω is the repetition frequency of the laser, whereas the second pump beam excites the sample at ω. By setting 575 nm pump beam to $\omega/2$, the experiment selects for the formation of new species that are formed following the second pump pulse. On the other hand, by setting the initial 420 nm pulse to $\omega/2$, the experiment selects for how the second pump at 575 nm modulates the population of the species formed intially with the 420 nm pulse. In both experiments, the repetition rate of the probe pulse is ω.[24,25]

Using the two-pump, one-probe spectroscopy with 575 nm set to $\omega/2$, transient absorption spectra were recorded after the arrival of the second pump as shown in Figure 5A. Immediately following excitation of ^{3*}PMI in ZnP−^{3*}PMI−*N*−NI, the transient absorption spectrum at 1 ps (Figure 5A, solid) shows features that are characteristic of a zinc porphyrin excited state, namely, absorption at 460−500 nm and bleaching at 550 and 600 nm. The broad absorption at 630−750 nm is probably due at least in part to a new excited state PMI species, since the excited states of zinc porphyrins absorb more weakly in this region. Gosztola et al.[14] showed that the transient absorption of PMI$^-$ contains a broad absorption feature from 630 to 750 nm. Given the similarities of the optical absorption spectra of excited states and radical anions within aromatic molecules, it is likely that the 630−750 nm feature in the 1 ps spectrum in Figure 5A is due to ^{3**}PMI. Transient absorption kinetics at 660 nm (not shown) shows that the 630−750 nm band appears with an instrument limited 150 fs time constant and decays with $\tau = 0.6$ ps. The absorption feature at 460 nm appears with $\tau = 0.6$ ps and decays with $\tau = 7$ ps to a longer-lived absorption, Figure 5B. This 7 ps time constant does not correlate with any processes observed in the one-pump−one-probe transient absorption experiment. The absorption bleach at 595 nm, Figure 5B, also recovers with $\tau = 7$ ps to a long-lived absorption. Since ^{3**}PMI decays with $\tau = 0.6$ ps, the transient absorption spectrum at 4 ps (Figure 5A, dotted) is composed mainly of the excited-state porphyrin formed in this two-pump experiment. Given that the magnitude of the absorption at 4 ps at 600−700 nm is very small and that the porphyrin excited state appears with a subpicosecond time constant, it is likely that ^{3*}ZnP is formed from ^{3**}PMI. The time constants for intersystem crossing in zinc porphyrins are on the order of nanoseconds, not picoseconds, so it is unlikely that ^{1*}ZnP could result from a reverse intersystem crossing mechanism. In summary, the spectral and kinetic data support the following mechanism:

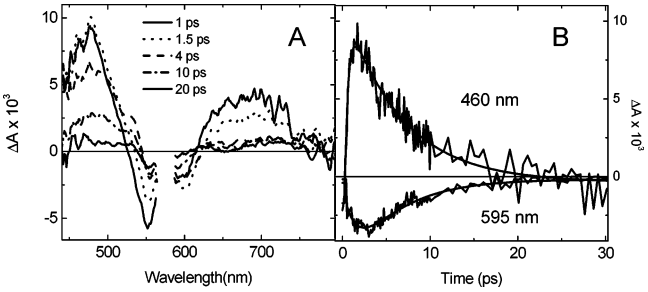

Figure 6. (A) Two-pulse−one-probe femtosecond spectra for ZnP−PMI−*N*−PI in toluene. The sample is excited at $t = 0$ with a 420 nm, 110 fs pulse at repetition frequency ω, followed by a second 575 nm, 110 fs pulse at $t = 3.5$ ns at repetition frequency $\omega/2$. The sharp negative feature at 575 nm due to scattered pump light was removed. (B) Transient absorption kinetics obtained at 460 and 595 nm. The abcissa gives the time following the 575 nm pulse.

$$\text{ZnP}-{}^{3**}\text{PMI}-N-\text{X} \xrightarrow{0.6\text{ ps}} {}^{3*}\text{ZnP}-\text{PMI}-N-\text{X} \xrightarrow{7\text{ ps}} \text{ZnP}-{}^{3*}\text{PMI}-N-\text{X}$$

The 7 ps TET time constant for ^{3*}ZnP to ^{3*}PMI cannot be measured using a one-pump−one-probe experiment due to the relatively slow rate at which ^{3*}ZnP is produced from ^{1*}ZnP.

One remaining issue is to explain the residual spectral features, which appear as ^{3*}ZnP disappears. The two-pump−one-probe transient absorption spectrum obtained 2 ns after the second 575 nm pump pulse, Figure 5A, matches the transient spectrum following one-pump excitation at 420 nm after a similar time frame. This is a consequence of the fact that some fraction of the energy in the second pump pulse is absorbed by molecules that do not contain ^{3*}PMI; that is, as expected, the initial 420 nm excitation does not produce a 100% yield of ZnP−^{3*}PMI−*N*−NI. Excitation of the remaining ground-state population of ZnP−PMI−*N*−NI with 575 nm light results in rapid singlet energy transfer from ^{1*}PMI to ZnP. The resultant population of ^{1*}ZnP undergoes the same photophysical processes that it does following 420 nm excitation alone, and thus, we see the appearance of the transient absorption features characteristic of the one-pump−one-probe experiment after the more rapid evolution of the features produced by the two-pump−one-probe sequence is complete.

The two-pump−one-probe transient absorption spectra and kinetics for ZnP−PMI−*N*−PI are shown in Figure 6. Using PI as an electron acceptor in this triad instead of NI makes it easier to identify whether an electron transfer mechanism occurs, since the PI radical anion absorbs strongly at 720 nm,[14] well-removed from all of the ZnP and PMI absorbance changes. The radical anion of NI primarily absorbs at 480 nm,[14] which overlaps significantly with the spectra of both ^{1*}ZnP and ^{3*}ZnP. Excitation of ^{3*}PMI in ZnP−PMI−*N*−PI followed the same timing sequence illustrated for ZnP−PMI−*N*−NI. We conclude that the reaction ZnP−^{3**}PMI−*N*−PI → ZnP−PMI−N^+−PI^- does not occur because the transient absorption spectra shown in Figure 6A do not show the sharp feature at 720 nm due to the presence of PI^-. The kinetic data presented in Figure 6B show once again that energy transfer from ^{3**}PMI to ZnP occurs in about 0.6 ps followed by TET from ^{3*}ZnP to PMI in about 7 ps. The two-pump−one-probe experiment on ZnP−PMI−*N*−PI shows that the transient spectrum nearly returns to $\Delta A = 0$ signifying that this two-step process is cyclic and returns the triplet energy back to PMI.

Two-Pump−One-Probe Nanosecond Transient Absorption Spectroscopy. Despite the fact that the one-pump, one-probe transient absorption experiment proves adequate to determine the relatively slow TET rate from ^{3*}ZnP to PMI in the ZnP−*N*−PMI−X compounds, we have carried out nanosecond two-pump, one-probe transient absorption spectroscopy on these compounds to determine whether the decay pathways for ^{3**}PMI within the ZnP−*N*−PMI−X compounds are similar to those observed for the ZnP−PMI−*N*−X compounds. For the two-pump−one-probe experiment, the second 532 nm pump pulse is set to $\omega/2$, which monitors the creation of new species as explained above for the femtosecond experiment. In the nanosecond experiment, excitation at 416 nm sensitizes the formation of ZnP−^{3*}*N*−PMI−X through the sequence: ^{1*}ZnP−*N*−PMI−X→ ^{3*}ZnP−*N*−PMI−X → ZnP−^{3*}*N*−PMI−X. Since the absorption maximum of ZnP−^{3*}*N*−PMI−X occurs at 540 nm, the 532 nm pulse serves well to excite ^{3*}PMI.

The transient absorption kinetics at 480 nm for both one and two-pump−one-probe experiments are similar for ZnP−*N*−PMI−PI, Figure 7A. This is reasonable because the 416 nm pulse at $t = 0$ occurs with frequency ω, whereas the second 532 nm pulse occurs with $\omega/2$, so that the transient absorption kinetics should be sensitive to processes induced by the second pump beam. However, a major amplitude difference is observed between the one- and two-pump experiments at 550 nm, Figure 7B, where the appearance of the ^{3*}PMI absorption occurs with $\tau = 55$ ns, yet does not recover to the ΔA value observed in the one-pump experiment. We can gain additional information by performing the corresponding two-pump experiment with the repetition frequency of the 416 nm pulse set to $\omega/2$, whereas that of 532 nm is ω. The transient kinetics are then sensitive to how the original population of ZnP−^{3*}*N*−PMI−X changes after the second pump pulse. Figure 8 shows the absorbance changes

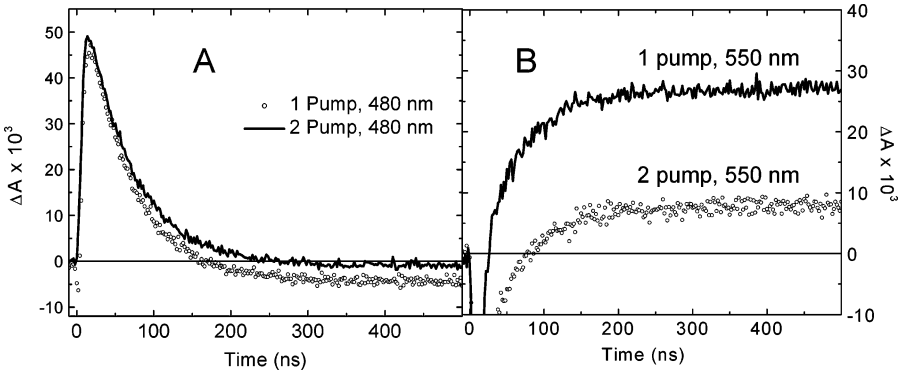

Figure 7. One- and two-pump nanosecond transient absorption kinetics of ZnP−*N*−PMI−PI in toluene at (A) 480 nm and (B) 550 nm. In the one-pump experiment, the sample is excited at $t = 0$ with a 416 nm, 7 ns pulse at repetition frequency $\omega/2$, whereas in the two-pump experiment, the sample is excited at $t = 0$ with a 416 nm, 7 ns pulse at repetition frequency ω followed by a second 532 nm, 7 ns pulse at $t = 90$ ns at repetition frequency $\omega/2$.

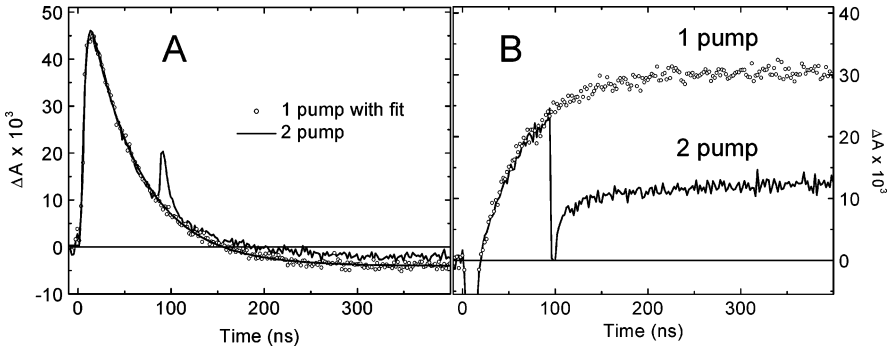

Figure 8. One- and two-pump nanosecond transient absorption kinetics of ZnP−*N*−PMI−PI in toluene at (A) 480 nm and (B) 550 nm. In the one-pump experiment the sample is excited at $t = 0$ with a 416 nm, 7 ns pulse at repetition frequency $\omega/2$, whereas in the two-pump experiment the sample is excited at $t = 0$ with a 416 nm, 7 ns pulse at repetition frequency $\omega/2$ followed by a second 532 nm, 7 ns pulse at $t = 90$ ns at repetition frequency ω.

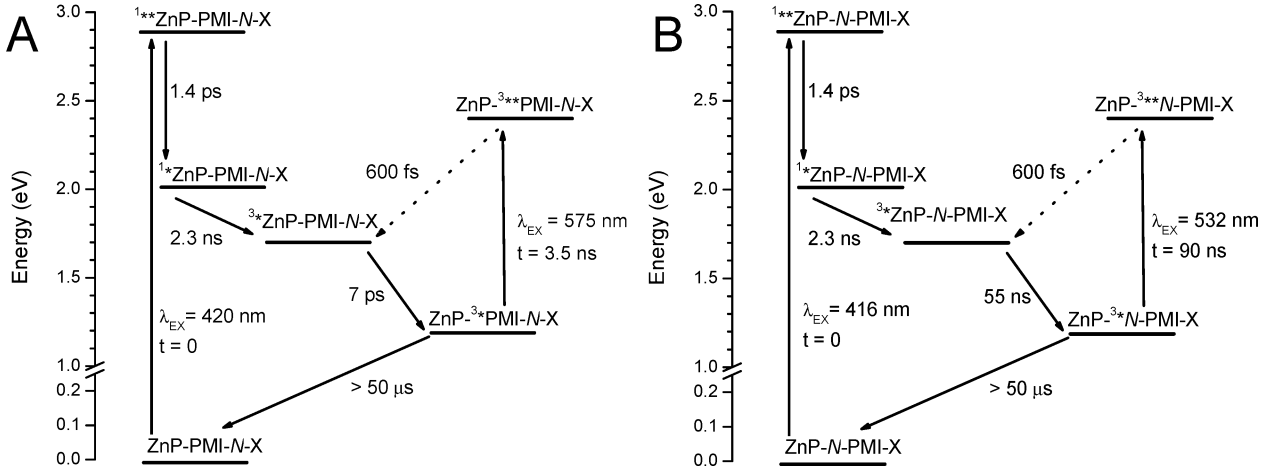

Figure 9. Energy level diagrams for (A) ZnP−PMI−*N*−X and (B) ZnP−*N*−PMI−X in toluene.

at 480 and 550 nm in which the second, 532 nm pump pulse arrives 90 ns after the first, 416 nm pump pulse. When the 532 nm pulse arrives at $t = 90$ ns, a further increase in the 480 nm absorption occurs, which subsequently decays with the normal 55 ns time constant, Figure 8A. Monitoring the formation of ^{3*}PMI at 550 nm in Figure 9B, the initial 416 nm laser pulse produces a population of ^{3*}PMI that increases with $\tau = 55$ ns until the second 532 nm pulse arrives at $t = 90$ ns. At that time, an immediate drop in ^{3*}PMI population occurs, which is followed by a biexponential recovery with $\tau_1 = 9$ ns and $\tau_2 = 55$ ns. The first component corresponds to the instrument response, whereas the second component is presumably the 55 ns formation of ^{3*}PMI by energy transfer from ^{3*}ZnP again. Once again, as was noted in Figure 7B, the population of ^{3*}PMI does not recover to the same ΔA value as observed for the corresponding one-pump experiment, Figure 8B. The data suggests that there is another deactivation channel for ZnP−$^{3**}N$−PMI−PI produced by the two-pump pulse sequence. This competitive channel may be rapid electron transfer: ZnP−$^{3**}N$−PMI−PI → ZnP−*N*−PMI^{+}−PI^{-} followed by charge recombination to ground state with a time constant faster than the 9 ns instrument response in this experiment. The strong electronic coupling expected for PI attached to the 9-position of PMI may make this electron-transfer process competitive with the TET: ZnP−$^{3**}N$−PMI−X → ^{3*}ZnP−*N*−PMI−X. TET should be slowed by the corresponding weak electronic coupling between ZnP and PMI through the N-imide. However, we cannot directly observe this hypothetical electron-transfer decay channel with our current apparatus because this measurement requires a two-pump−one-probe experiment with the two pump pulses having approximately a 100 ns delay between them and, at the same time, having at least picosecond time resolution to monitor the formation and decay of species produced following the second pump pulse.

Nevertheless, we can estimate the rate of the electron-transfer reaction, ZnP−$^{3**}N$−PMI−PI → ZnP−*N*−PMI^{+}−PI^{-}, by measuring the rate of the analogous singlet state reaction in the model system, PI−PMI−*N*−*t*-Bu$_2$Ph. One-pump−one-probe transient absorption measurements on this model system in toluene using 540 nm photoexcitation yields charge separation and recombination time constants of $\tau_{CS} = 25$ ps and $\tau_{CR} = 970$ ps, respectively. Since our spectroscopic measurements show that the energies of the $S_0 \rightarrow S_1$ transition of PMI and the $T_1 \rightarrow T_n$ transition in ^{3*}PMI are similar, we assume that the free energies of reaction for the charge separation reactions, *t*-Bu$_2$Ph−$^{1*}N$−PMI−PI → *t*-Bu$_2$Ph−*N*−PMI^{+}−PI^{-} and ZnP−$^{3**}N$−PMI−PI → ZnP−*N*−PMI^{+}−PI^{-}, are also similar. Thus, it is likely that electron-transfer reaction sequence, ZnP−$^{3**}N$−PMI−PI → ZnP−*N*−PMI^{+}−PI^{-} → ZnP−*N*−PMI−PI, is complete on the order of 1 ns, so that the nanosecond two-pump experiment cannot resolve this additional possible deactivation channel for ^{3**}PMI. We only observe a net loss in ^{3*}PMI population due to competition of the electron-transfer reaction: ZnP−$^{3**}N$−PMI−PI → ZnP−*N*−PMI^{+}−PI^{-} with TET: ZnP−$^{3**}N$−PMI−PI → ^{3*}ZnP−*N*−PMI−PI. The energy level diagram presented in Figure 9 summarizes the results of our experiments.

Electronic Coupling and Triplet Energy Transfer Rates. The large differences in triplet energy transfer rates to PMI as a function of the attachment site of the ZnP energy donor stem

from the fact that TET takes places via an electron−electron exchange interaction, the so-called Dexter mechanism, in which simultaneous hole and electron transfer take place to transfer triplet energy.[19,20] The electronic coupling matrix element for TET between two chromophores is directly proportional to the product of their electronic coupling matrix elements for electron and hole transfer:

$$V^{TT} \propto V^{ET}V^{HT} \quad (1)$$

Closs et al.[21,32] examined TET from benzophenone to naphthalene and electron transfer from biphenyl to naphthalene attached to cyclohexane and decalin spacers. They showed that TET can be modeled as a double electron transfer and verified eq 1. Similarly, we expect to see larger changes in rates for TET versus individual electron/hole transfer rates as we change the attachment site of ZnP to PMI. When our molecules are dissolved in toluene, the free energies of reaction for electron transfer from ^{1*}ZnP to PMI are positive, so that electron transfer does not compete with ISC of the zinc porphyrin. However, we have observed electron transfer from ^{1*}ZnP to PMI, when the molecules are dissolved in the more polar solvent 2-methyltetrahydrofuran. The time constants for photoinduced charge separation and recombination within ZnP−*N*−PMI−H are τ_{CS} = 330 ps and τ_{CR} = 920 ps, respectively, which are obtained by monitoring the formation of PMI^- at 620 nm.[13] On the other hand, the corresponding time constants for ZnP−PMI−*N*−(*t*-Bu_2Ph), are τ_{CS} = 14 ps and τ_{CR} = 72 ps, respectively. The electron-transfer rates for ZnP−PMI−*N*−X in which the ZnP donor is attached to the 9-position of the PMI acceptor are more than an order of magnitude faster than those for ZnP−PMI−*N*−X in which ZnP is attached to PMI at its imide nitrogen atom. These data support the idea that the electronic coupling matrix element for electron transfer through the 9 position of PMI is larger than that for the imide nitrogen position. Thus, it is likely that the large difference observed for the TET rates from ^{3*}ZnP to PMI as a function of their position of attachment is due to the multiplicative effect of the electronic coupling matrix elements for hole and electron-transfer reflected by eq 1.

This large difference in TET rates is an extreme case of what has been observed for singlet−singlet energy transfer within covalently linked porphyrin dyads. It was found that the rate of singlet energy transfer within the dyads depends on whether the porphyrins are attached to the linker group by their meso or β positions.[33−38] In addition, it was found that changing the electron density at the porphyrin positions attached to the linker using substituents on the porphyrins changes the singlet energy transfer rate. The difference in singlet energy transfer rate between two porphyrins attached to a diphenylethynyl linker group by their meso positions versus that between one porphyrin with a *meso* attachment to the linker and a second porphyrin with a β attachment to the same linker ranges from 2 to 10 depending on other substituents on the porphyrins. Both effects are a consequence of the fact that the two highest occupied molecular orbitals of porphyrins have a_{1u} and a_{2u} symmetry. It is well-known that the a_{1u} orbital has significant electron density at the β carbons of the porphyrin with little density at the meso positions, whereas the opposite is true for the a_{2u} orbital.[38,39] Which of these two orbitals is the porphyrin HOMO depends on the nature and the position of the substituents attached to the porphyrin. For example, when the meso positions (5,10,-15,20) of the porphyrin are substituted with electron-donating groups, e.g., phenyl rings or alkyl chains, the a_{2u} orbital is the HOMO. On the other hand, substitution of the β positions with electron releasing groups, such as alkyl groups, results in the a_{1u} orbital being the HOMO. Generally, increased electron density at particular peripheral carbon atoms of the porphyrin results in stronger electronic coupling to molecules attached to those positions. If the attached molecule can accept energy and/or electrons from the porphyrin, the increased electronic coupling generally leads to increased rates of energy and/or electron transfer.[37]

Conclusions

We have shown that a three-pulse (two-pump, one-probe) transient absorption experiment reveals rates of TET that a one-pump experiment cannot. The triplet energy transfer rate constant of $(7\ ps)^{-1}$ for ^{3*}ZnP−PMI−*N*−X → ZnP−^{3*}PMI−*N*−X is due to the strong electronic coupling of the excited state of PMI and ZnP through the 9-position of PMI. We have also shown that the TET rate for ^{3*}ZnP−*N*−PMI−X → ZnP−^{3*}*N*−PMI−X through the N-imide of PMI is over 8000 times slower $(55\ ns)^{-1}$. These large changes in TET rates are a consequence of the TET mechanism, which reflects the large differences between the HOMO and LUMO coefficients at the 9 position of PMI and that for its imide nitrogen atom. The ability to tune TET rates to PMI by a judicious choice of structural changes will be helpful in developing strategies for molecular based electronics and light harvesting arrays with porphyrins.

Acknowledgment. This work was supported by the National Science Foundation (CHE-0102351) and the Office of Naval Research (N00014-02-1-0381).

Supporting Information Available: Syntheses of the molecules shown in Figure 1. A detailed explanation and illustration of the data collection for the two-pump nanosecond experiment. This material is available free of charge via the Internet at http://pubs.acs.org.

References and Notes

(1) Ermolaev, V. L. *Russ. Chem. Rev.* **2001**, *70*, 471−490.
(2) Turro, N. J.; Ramamurthy, V.; Cherry, W.; Farneth, W. *Chem. Rev.* **1978**, *78*, 125−145.
(3) McGimpsey, W. G. *Trends Org. Chem.* **1997**, *6*, 233−257.
(4) McGimpsey, W. G. *Mol. Supramol. Photochem.* **1998**, *2*, 249−306.
(5) Johnston, L. J. *Chem. Rev.* **1993**, *93*, 251−266.
(6) Scaiano, J. C.; Johnston, L. J. In *Organic Photochemistry*; Padwa, A., Ed.; Marcel Dekker: New York, 1989; Vol. 10, p 309.
(7) Lukas, A. S.; Wasielewski, M. R. In *Electron Transfer in Chemistry*; Balzani, V., Ed.; Wiley-VCH: New York, 2001; Vol. 5, pp 48−96.
(8) Ambroise, A.; Kirmaier, C.; Wagner, R. W.; Loewe, R. S.; Bocian, D. F.; Holten, D.; Lindsey, J. S. *J. Org. Chem.* **2002**, *67*, 3811−3826.
(9) Tomizaki, K.; Loewe, R. S.; Kirmaier, C.; Schwartz, J. K.; Retsek, J. L.; Bocian, D. F.; Holten, D.; Lindsey, J. S. *J. Org. Chem.* **2002**, *67*, 6519−6534.
(10) Yang, S. I.; Lammi, R. K.; Prathapan, S.; Miller, M. A.; Seth, J.; Diers, J. R.; Bocian, D. F.; Lindsey, J. S.; Holten, D. *J. Mater. Chem.* **2001**, *11*, 2420−2430.
(11) Just, E. M.; Wasielewski, M. R. *Superlattices Microstruct.* **2000**, *28*, 317−328.
(12) Fuller, M. J.; Wasielewski, M. R. *J. Phys. Chem. B* **2001**, *105*, 7216−7219.
(13) Hayes, R. T.; Wasielewski, M. R.; Gosztola, D. *J. Am. Chem. Soc.* **2000**, *122*, 5563−5567.
(14) Gosztola, D.; Niemczyk, M. P.; Svec, W. A.; Lukas, A. S.; Wasielewski, M. R. *J. Phys. Chem. A* **2000**, *104*, 6545−6551.
(15) Gosztola, D.; Niemczyk, M. P.; Wasielewski, M. R. *J. Am. Chem. Soc.* **1998**, *120*, 5118−5119.
(16) Miller, S. E.; Zhao, Y.; Schaller, R.; Mulloni, V.; Just, E. M.; Johnson, R. C.; Wasielewski, M. R. *Chem. Phys.* **2002**, *275*, 167−183.

(17) Mercadante, R.; Trsic, M.; Duff, J.; Aroca, R. *THEOCHEM* **1997**, *394*, 215−226.

(18) The semiempirical PM3 method implemented in HyperChem(TM) (Hypercube, Inc., 1115 NW 1114th Street, Gainesville, FL 32601, USA) was used to calculate the energy-minimized structure of 1,6-diphenoxy-PMI with a hydrogen atom attached to its imide nitrogen atom.

(19) Piotrowiak, P. In *Volume 1: Principles, Theories, Methods, and Techniques*; Piotrowiak, P., Ed.; Wiley-VCH: New York, 2001; Vol. 1, pp 215−237.

(20) Dexter, D. L. *J. Chem. Phys.* **1953**, *21*, 836−850.

(21) Closs, G. L.; Calcaterra, L. T.; Green, N. J.; Penfield, K. W.; Miller, J. R. *J. Phys. Chem.* **1986**, *90*, 3673−3683.

(22) Giaimo, J. M.; Gusev, A. V.; Wasielewski, M. R. *J. Am. Chem. Soc.* **2002**, *124*, 8530−8531.

(23) Greenfield, S. R.; Svec, W. A.; Gosztola, D.; Wasielewski, M. R. *J. Am. Chem. Soc.* **1996**, *118*, 6767−6777.

(24) Debreczeny, M. P.; Svec, W. A.; Wasielewski, M. R. *Science* **1996**, *274*, 584−587.

(25) Debreczeny, M. P.; Svec, W. A.; Wasielewski, M. R. *New J. Chem.* **1996**, *20*, 815−828.

(26) Ebbesen, T. W. *New J. Chem.* **1991**, *15*, 191−198.

(27) Gouterman, M. *The Porphyrins*; Academic Press: New York, 1978; Vol. III.

(28) Kadish, K. M.; Shiue, L. R. *Inorg. Chem.* **1982**, *21*, 3623−3630.

(29) Reed, R. A.; Purrello, R.; Prendergast, K.; Spiro, T. G. *J. Phys. Chem.* **1991**, *95*, 9720−9727.

(30) Pekkarinen, L.; Linschitz, H. *J. Am. Chem. Soc.* **1960**, *82*, 2407−2411.

(31) Harriman, A. *J. Chem. Soc., Faraday Trans. 2* **1981**, *77*, 1281−1291.

(32) Closs, G. L.; Piotrowiak, P.; Maclnnis, J. M.; Fleming, G. R. *J. Am. Chem. Soc.* **1988**, *110*, 2652−2653.

(33) Osuka, A.; Tanabe, N.; Kawabata, S.; Yamazaki, I.; Nishimura, Y. *J. Org. Chem.* **1995**, *60*, 7177−7185.

(34) Strachan, J.-P.; Gentemann, S.; Seth, J.; Kalsbeck, W. A.; Lindsey, J. S.; Holten, D.; Bocian, D. F. *J. Am. Chem. Soc.* **1997**, *119*, 11191−11201.

(35) Balasubramanian, T.; Lindsey, J. S. *Tetrahedron* **1999**, *55*, 6771−6784.

(36) Yang, S. I.; Seth, J.; Balasubramanian, T.; Kim, D.; Lindsey, J. S.; Holten, D.; Bocian, D. F. *J. Am. Chem. Soc.* **1999**, *121*, 4008−4018.

(37) Holten, D.; Bocian, D. F.; Lindsey, J. S. *Acc. Chem. Res.* **2002**, *35*, 57−69.

(38) Fajer, J.; Borg, D. C.; Forman, A.; Dolphin, D.; Felton, R. H. *J. Am. Chem. Soc.* **1970**, *92*, 3451−3459.

(39) Weiss, C.; Kobayashi, H.; Gouterman, M. *J. Mol. Spectrosc.* **1965**, *16*, 415−450.